SUPERSONIC FLOW IN A CONVERGENT-DIVERGENT NOZZLE

Jason Garza*, Kortny Hall†, and Ed Marks‡
Department of Aerospace and Mechanical Engineering
University of Notre Dame
Notre Dame, IN 46556

May 2, 2001

Abstract

An experiment examining the flow through a convergent-divergent nozzle at various back pressures is presented. An in-draft supersonic wind tunnel ran and resulted in the following flow regimes: subsonic, choked throat, choked throat with a shock downstream, and a choked throat with a shock beyond the exit plane. Also, a pitot tube and two different cones were set in the flow, and the resulting shock waves were analyzed. The Mach numbers determined from pressure data at various points in the tunnel were compared with the Mach numbers estimated by measuring wave angles. A schlieren flow visualization system was utilized to capture images of the shock waves. The expected trends that resulted from variations of back pressure were seen, and data matched closely with theory.

Nomenclature

M = Mach number
P = pressure
P_b = back pressure
P_e = exit pressure
T = temperature
V = velocity
e_x = error in quantity x
x^* = value of quantity x at Mach 1
β = wave angle
δ = deflection angle
γ = ratio of specific heats
ρ = density

Introduction

There have been many goals explored to understand the physics and aerodynamics of flight since man has become airborn. Some aimed to fly higher, others desired to fly with more stealth, and yet others desired to fly more efficiently, but one of the most prevalent goals of flight research has been to achieve higher flight velocities. Since the Wright brothers took the first step and launched what has been nearly a century's worth of flight and research, people have sought to fly at speeds faster than man has ever traveled before. As research continued to develop, the speeds that aircraft were able to reach increased steadily until an aerodynamic phenomenon was encountered at speeds approaching the speed of sound. However, once that barrier of surpassing the speed of sound was overcome, the speeds have continued to rise.

Coming into and during World War II, planes were approaching the speed by which sound travels through air. Since the war called for faster and faster planes, the British government began to compete with the Germans to be the first to break the sound barrier. As the two sides competed, planes and their pilots began to approach the sound barrier, Mach 1, but could never break it due to strange phenomena that occurred as they approached the higher speeds. The plane's stability would decrease and the pilots would lose control of their equipment. Eventually, the British government involved the United States in its search for answers, and it was discovered that the reason things were unpredictable near Mach 1 was due to a new kind of drag being encountered called wave drag. As air moving over a plane's wing approaches the speed of sound, a shock wave forms and the experienced drag increases significantly. Also, the flight controls began to fail because when operating behind a shock wave, the flight controls do not have any influence over the flow before the shock wave, resulting in less control of the aircraft.

Though the war ended, the sound barrier remained and the race to break it continued. In Muroc Dry Lake Bed, California, that barrier was broken by an ex-fighter pilot turned test pilot, Captain Chuck Yeager. With that historic flight on October 14, 1947, the sound barrier crumbled and supersonic flight emerged as the faster way to travel. After that flight, the race to fly faster continued and Capt. Yeager continued to fly faster than anyone else.[1]

As research improved the understanding of supersonic flight, the move towards hypersonic speeds progressed. Now in the 21st century, hypersonic travel is possible as the new X-43 is being prepared for flight at the NASA Dryden Flight Research Center. The X-43, shown in Fig. 1, is scheduled to fly at Mach 7 on May 19, 2001.[2]

*Undergraduate, Student Member AIAA.
†Undergraduate, Student Member AIAA.
‡Undergraduate, Vice President AIAA.

Figure 1: An Artist Rendition of the X-43 in Flight.[2]

With the expense of many lives lost trying to break the sound barrier into hypersonic flight, knowledge of shock waves has increased flight velocities since the Wright brothers. Shock waves occur at the point were supersonic flow immediately slows to a subsonic speed. The sudden decrease in velocity is accompanied by a pressure, temperature, and density rise across the shock wave.

Within the remainder of this report, fundamental principles of de Laval nozzles will be presented, as well as an experiment involving some basic elements of shock waves. Pictures of shock waves at the throat of the nozzle and in the divergent section, as well as around a pitot tube and two cones will be analyzed. A discussion of the findings will detail the Mach numbers found from the pressure measurements and compare these results with the estimated Mach numbers based on the wave angles. An uncertainty analysis will conclude the report.

Background

Normal Shock Waves

In supersonic flow, the extremely thin region in which transition from supersonic, low pressure flow to subsonic, high pressure flow occurs is known as a shock wave. As the name suggests, a normal shock wave occurs when the flow upstream and downstream of the shock are at right angles to the shock. Normal shock waves can occur, for example, in the intakes of engines on supersonic aircraft, in the exhaust system of reciprocating engines, in gas pipelines, and in mine shafts due to explosions.

Normal shock waves can be either stationary or moving. Stationary shock waves typically occur in a steady flow, while moving shock waves are generated by sudden disturbances in a flow. Shock waves form in a similar fashion to sound waves. Pressure disturbances expand outward from an object at the speed of sound. If, for example, an airplane was flying supersonically, the disturbances caused by the plane propagating at the speed of sound would "catch up" to one another, but could not pass through each other. This building up of pressure disturbances creates a shock wave. Large pressure and temperature jumps are experienced across a shock wave. A pitot tube positioned in a supersonic flow produces a common example of a modeled shock. In that case a normal shock wave is assumed to act in the region directly upstream of the pitot tube.

The equation relating the Mach numbers before and after a normal shock wave is shown below.

$$\frac{M_2}{M_1} = \frac{\left(1 + \frac{(\gamma-1)}{2} M_2^2\right)^{\frac{\gamma+1}{2(\gamma-1)}}}{\left(1 + \frac{(\gamma-1)}{2} M_1^2\right)} \tag{1}$$

Eqn. 1 is interesting in that it shows that the Mach number downstream of a normal shock is dependent only on the upstream Mach number. Similar equations show that the pressure and temperature jumps across a shock are also functions of only the Mach numbers.

Oblique Shock Waves

Oblique shock waves are analyzed just as normal shock waves, but only the normal component of velocity to the shock is important. There are no changes in the flow variables in the direction parallel to the wave, and subsequently there is no net force and no momentum change parallel to the wave. Once the system is reduced to a normal shock case, normal shock relations are used to analyze the flow.

Oblique shocks form when a flow is turned. This can result from flow over a wedge or cone, or if a tunnel wall turns through an angle. The resultant shock wave forms at an angle β to the original flow, and the flow is turned through the angle δ of the cone or wedge. In the case of this experiment, the Mach number of the flow could be determined by measuring this angle β that was captured through the schlieren visualization technique. With the cone angle known, the relation between deflection angle, shock angle, and local Mach number is

$$\tan\delta = \frac{(M_x^2 \sin^2\beta - 1)(\cot\beta)}{\frac{\gamma+1}{2} M_x^2 - M_x^2 \sin^2\beta + 1}. \tag{2}$$

Convergent-Divergent Nozzles

Convergent-divergent nozzles, also known as de Laval nozzles, are used to create supersonic flow for a

myriad of applications. Not only are they useful for wind tunnel experiments, but in the real world they are widely used in jet engines of supersonic aircrafts, exhaust nozzles of motors, and inlets of turbines. The behavior of the flow through a convergent-divergent nozzle is dependent on the ratio of back pressure P_b to inlet pressure P_0. As back pressure decreases, the flow can be characterized as one of four basic flow regimes.

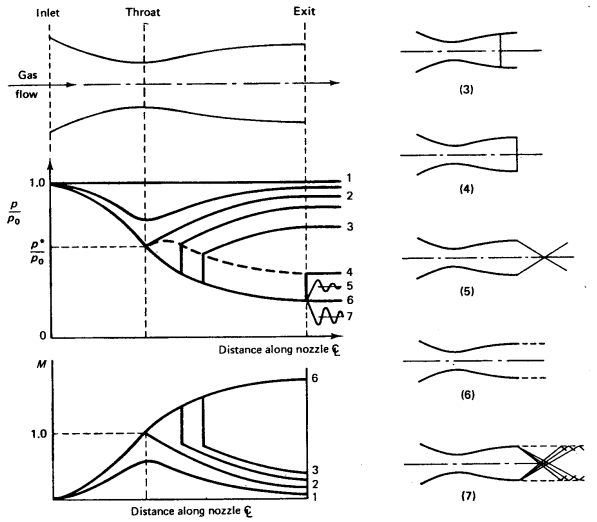

Figure 2: Effect of Back Pressure on C-D Nozzle Flow.[3]

When the ratio of P_b/P_0 is very close to one, the flow remains subsonic throughout the nozzle. The flow in the nozzle is then similar to that in a venturi. The pressure drops to a minimum value at the nozzle throat which is greater than P^*, and then increases in the divergent section of the nozzle until it is equal to the original pressure P_0. In this type of system, the mass flow rate can be increased by decreasing the back pressure. This is illustrated in Case 1 of Fig. 2. Case 1 also illustrates the subsonic flow throughout the nozzle. As the flow contracts through the throat, the Mach number increases to a maximum value that is less than one. As the flow then expands, it slows down because the nozzle is not choked.

As the back pressure is lowered, it will eventually reach a value at which the throat pressure becomes equal to the critical pressure and the Mach number at the throat is equal to one. This back pressure, referred to as $P_{b,crit}$, is the pressure at which the throat pressure first drops to its critical value. Once the Mach number at the throat is equal to one, further reductions in the back pressure cannot affect conditions upstream of the throat and cannot alter the mass flow rate through the nozzle. The nozzle is said to be choked once the back pressure has been reduced to $P_{b,crit}$. This second flow regime is shown in Case 2 in Fig. 2.

As the back pressure is reduced below $P_{b,crit}$, supersonic flow develops downstream of the nozzle. This region of supersonic flow is terminated by a normal shock wave. This shock wave increases the pressure and reduces the velocity to a subsonic value. Since the flow is then subsonic, the diverging nozzle causes it to decelerate until the exit pressure is equal to the back pressure. This is illustrated in Case 3 of Fig. 2. Although it is not always the case that the shock in the divergent section of the nozzle is entirely normal, it is typically modeled as such.

If the back pressure is further reduced, the shock wave in the divergent section will move towards the exit plane. Eventually the back pressure will be such that the shock is located directly at the exit. The flow is again isentropic throughout until the shock wave is reached. This regime is illustrated in Case 4 of Fig. 2. The normal shock will disappear if the back pressure is reduced past this value, and a series of oblique shocks form outside of the exit of the nozzle. Further reductions in the back pressure will result in the nozzle operating at its design condition when P_b becomes equal to P_e. This means that there are no shocks anywhere in the system and that the flow is isentropic throughout. This is shown in Case 6 of Fig. 2.

Schlieren Method

Although there are various methods used to visualize density changes in liquids and gases, the schlieren system is very effective and often used for teaching situations. This system was first introduced in the 1950s, and it is at times preferable over other methods of flow visualization, such as interferometric techniques for example, because of its relatively easy setup and low cost. Using a broad light source rather than a small or point source, a series of mirrors reflect the light through a region in which density is changing and projects an image onto a screen which can easily be viewed. This system takes advantage of the fact that the index of refraction of a fluid varies with density.

In compressible supersonic flow, shock waves are examples of regions in which there exists a significant density gradient. The schlieren system utilizes a beam of collimated light that is passed through the test section. A knife edge is placed at the focal points of the spherical mirrors to block out a fraction of the reflected light. This allows the intensity of the image on the screen to be controlled. As the beam of light passes through the flow, it is deflected by an amount that is proportional to the spatial density gradient. Within the deflected beam, some of the rays are bent far enough so as not to be deflected by the knife edge. The resulting image is a light projection with dark areas that correspond to regions of different density, specifically shock waves, expansion waves, and bound-

ary layers. An illustration of the schlieren system used in this experiment can be found in Fig. 3.

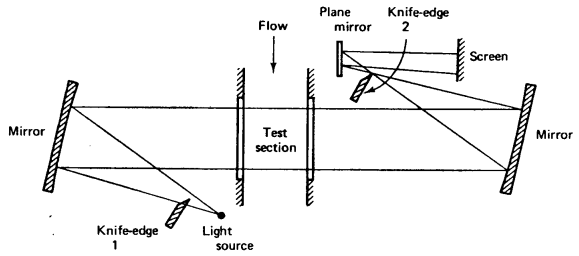

Figure 3: Schlieren System.[3]

Experimental Facilities

Figure 4: Supersonic In-Draft Wind Tunnel Setup.

This experiment was performed in the main laboratory and test facility in the Hessert Center for Aerospace Research at The University of Notre Dame. A supersonic in-draft wind tunnel, shown in Fig. 4, was used to create the desired flow rates. The tunnel was driven by a 93.2 kW, 0.0283 m^3/min vacuum pump. This pump drew in air from the room through a de Laval nozzle, a convergent-divergent nozzle which allowed for speeds of M = 1 and higher. After the air flowed through the test section, it diffused and flowed into the vacuum pumps. The geometry of the supersonic tunnel is described in Fig. 5 and a schematic is shown in Fig. 6.

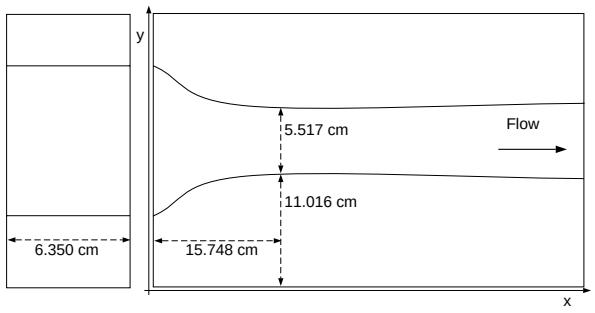

Figure 5: Nozzle Geometry.

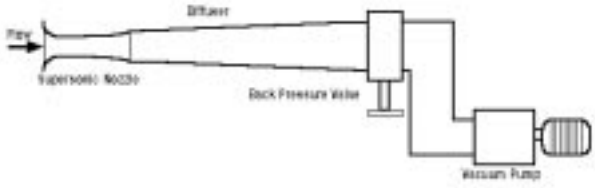

Figure 6: Supersonic Wind Tunnel Schematic.[3]

To measure pressure along the nozzle, a multi-tube mercury manometer was used. The position of the static pressure holes is given in Table 1.

A schlieren flow visualization system was used to project a visible image of the shocks in the tunnel. This system is an extremely effective method of viewing shock waves, as it takes advantage of the fact that the index of refraction of a fluid varies with its density. For this experiment, light was reflected by a spherical mirror through the test section, and another spherical mirror reflected this image through a system of a knife edge and plane mirror onto the viewing screen.

A pitot probe and two different cones with a half-angle δ of 14° were used to create oblique shocks in the test section. The schlieren images of these shocks, as well as the normal shocks that were formed in the tunnel due to various settings of back pressure, were captured using a Kodak digital camera.

Experimental Procedure

The static pressure and temperature in the lab were measured to be 98.5 $\pm$ 0.0067 kN and 25 $\pm$ 0.5°C, respectively. The wind tunnel was operated at four different back pressures, with each P_b resulting in a different

Tap #	x (cm)
1	8.128
2	9.398
3	10.668
4	14.478
5	15.113
6	15.748
7	16.383
8	17.018
9	17.653
10	18.288
11	19.558
12	20.828
13	22.098
14	25.908
15	27.178
16	28.448
17	29.718
18	30.988

Table 1: Position of Pressure Taps Along the Nozzle.

flow regime. The ratio P_b / P_0 was set such that the tunnel operated at the following conditions: subsonically, M_{throat} = 1 with a normal shock standing in the throat, M_{throat} = 1 with the normal shock downstream of the throat, and at the design condition, which corresponds to the flow being isentropic throughout.

For each of the four back pressures, the schlieren system was utilized to observe the flow. Digital photographs were taken for each flow regime, and the shocks that were present in the tunnel could be seen on the screen. Also, for each back pressure, measurements were taken at the pitot tube and at each of the pressure taps using a multi-tube mercury manometer. This technique illustrated quite clearly where any large jumps in pressure took place, which corresponded to the presence of a shock wave.

With the tunnel operating at its design condition, a cone model was mounted in the tunnel. Again using the schlieren flow visualization technique, the flow around the cone was observed, specifically the formation and location of oblique shocks. From the photographs, the shock angles could be measured, and from these, the Mach number could be determined. The cone had a half angle of 14°. Another smaller cone of the same half angle was tested with the tunnel operating at its design condition, and the resulting oblique shock waves were analyzed in a similar fashion. Finally, a total static tube with a built-in type K thermocouple was inserted into the test section, and for several back pressures, measurements of total pressure and temperature were taken.

Results and Discussion

In Fig. 7 and Fig. 8, the theoretical and measured values of the local Mach number and local pressure to static pressure ratios are shown plotted against the length of the nozzle.

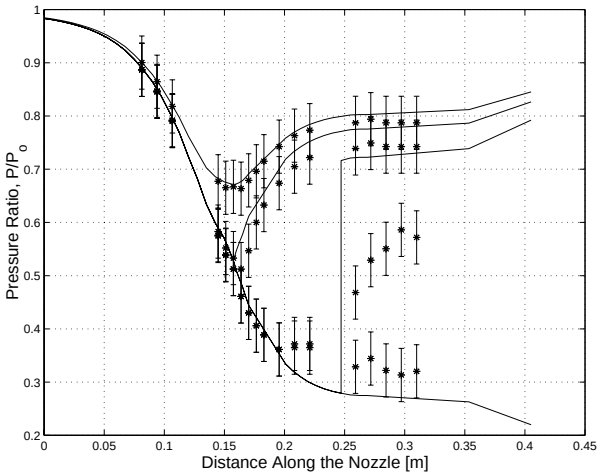

Figure 7: Pressure Ratio vs. Nozzle Length.

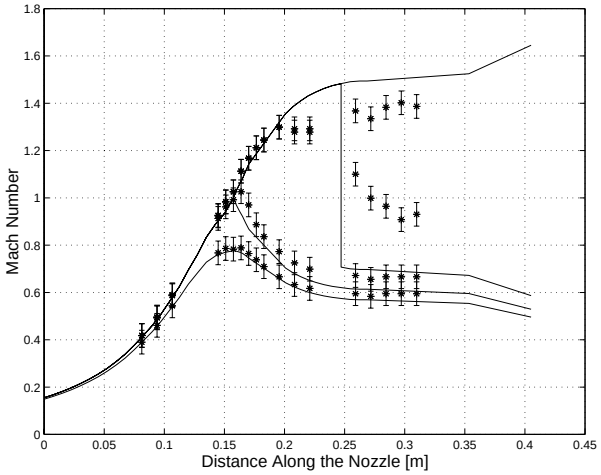

Figure 8: Mach Number vs. Nozzle Length.

The first flow is subsonic throughout. It speeds up while the nozzle converges, but without reaching the sonic condition, it then slows back down past the throat. The second condition shown is the next line from the completely subsonic. Here, the flow is sped up through the converging section of the nozzle to the sonic condition at the throat, where after passing through a normal shock at the throat, it slows down as the remainder of the

nozzle diverges. The third condition is the supersonic design condition. Like the subsonic design condition, the flow speeds up to $M = 1$ at the throat, but then continues to speed up through the diverging section to the exit. The last flow condition shown represents the flow through the nozzle with a shock wave in the diverging section. Until the shock wave, this flow follows that of the supersonic design condition. After the shock wave, however, the pressure jumps with a large pressure rise across the shock and the Mach number slows to a subsonic value. After going through the shock wave, the now subsonic flow continues to slow down to the exit.

In the following subsections, each of these flows will be considered individually.

Completely Subsonic

Fig. 9 and Fig. 10 show the completely subsonic case only, which was referred to above.

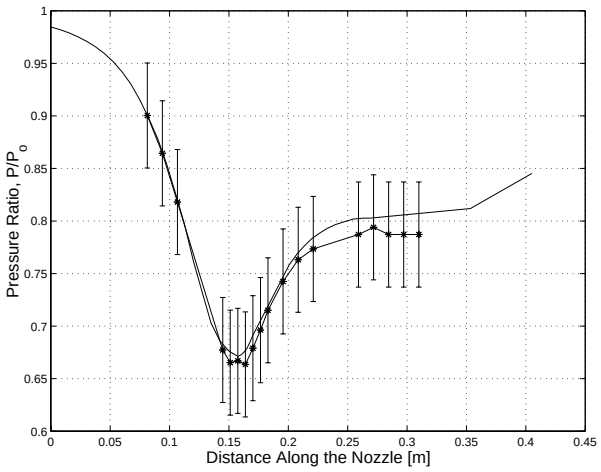

Figure 9: Pressure Ratio vs. Nozzle Length.

It can be seen that the measured values follow the theoretical line very closely, especially in the converging section of the nozzle. However, as the flow approaches the exit in the diverging portion of the nozzle, the pressure ratio is lower and the Mach number is higher than theory predicts. This comes as a result of the boundary layers developing on the surface of the nozzle. As the boundary layer develops, the area that the flow has to move through is actually smaller than the cross-sectional area of the nozzle. Since theory ignores these effects of the boundary layers, it predicts values based on the entire cross-sectional area of the nozzle. Thus, because the actual area that the flow is moving though is smaller than the one taken into account by theory, the pressure will be lower and the Mach number will be higher than theoretical predictions. Even with the boundary layers

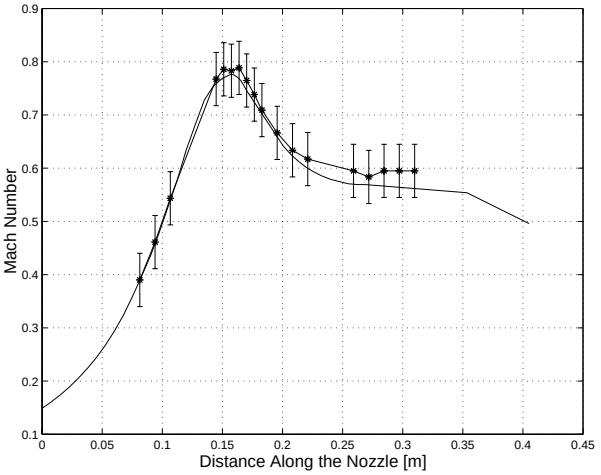

Figure 10: Mach Number vs. Nozzle Length.

though, the discrepancies are small and the measured results match well with theory.

It should be noted that the Mach number at the exit, or the last tap, can be calculated two different ways using the pressure tap at this point. For these operating conditions, the pressure tap gives $M_e = 0.60$ using a pressure ratio along with tabulated data,[4] and $M_e = 0.595$ using the isentropic flow relations. The theoretically predicted value is $M_e = 0.562$. Both methods of calculating M_e from the pressure tap data are reasonably similar and in agreement with one another to a value that is higher than the theoretically predicted one. However, as previously discussed, theory does not take into account boundary layers and results in an actual M_e that is higher than expected.

Shock Wave in the Throat

Fig. 11 and Fig. 12 show the shock wave in the throat only, which was referred to above.

Even thought there is a shock occurring in the flow, the flow is still very similar to that at the subsonic design condition. With the shock at the throat, the flow has very little time to speed up past $M = 1$ before it returns to subsonic conditions.

As was the case in the completely subsonic flow, the diverging values of the measured quantities after the throat are slightly different than the theoretically predicted values. The reasons for this are similar to the completely subsonic case as the boundary layer affects the flow in the diverging section of the nozzle.

It also should be noted that the sonic condition, and thus the throat, actually takes place at a point between the geometric throat and the pressure tap one spot behind it. This occurs for similar reasons as the discrepancies described above. Caused by the boundary layer

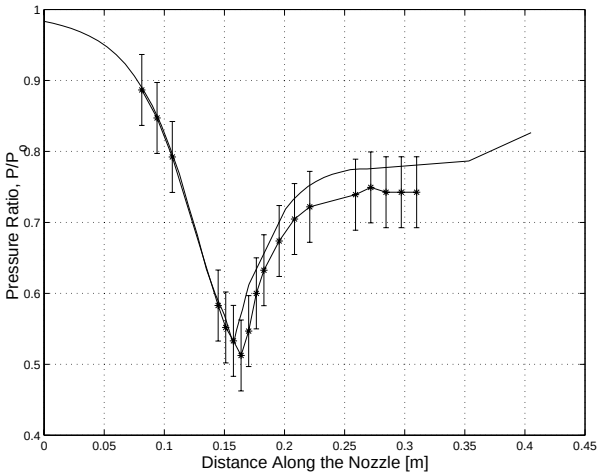

Figure 11: Pressure Ratio vs. Nozzle Length.

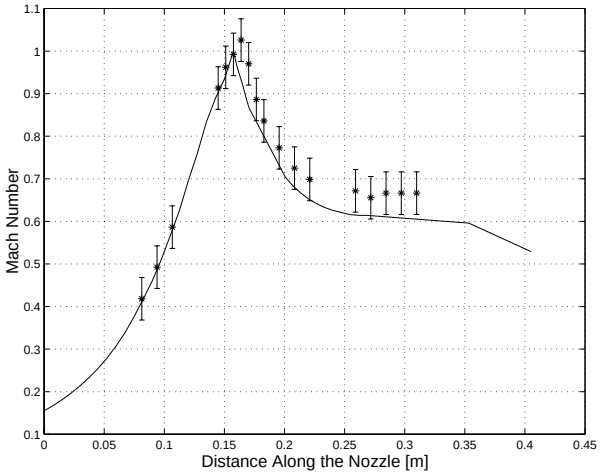

Figure 12: Mach Number vs. Nozzle Length.

growth, the area of the nozzle just behind the throat is actually smaller as far as the flow is concerned than the area at the geometric throat. Again, theory does not take this boundary layer into account, and as a result, has the sonic condition occurring at the geometric throat before the flow slows down.

Fig. 13 shows the shock wave occurring at the throat. Just right of center in this picture, the shock can barely be made out. Because the changes across this shock are small, the representation of them using schlieren techniques is not very good. By what can be made out of the shock, especially at the edges, it can be reasonably confirmed that the shock is indeed a normal shock wave.

As for M_e, the two methods of calculating M_e using the last pressure tap results in $M_e = 0.67$ and $M_e = 0.666$. Compared to theory, $M_e = 0.608$, the

Figure 13: Shock Wave at the Nozzle Throat.

measured values are high, but similar to before, this is reasonable.

Supersonic Design Condition

Fig. 14 and Fig. 15 show the previously mentioned supersonic design condition only.

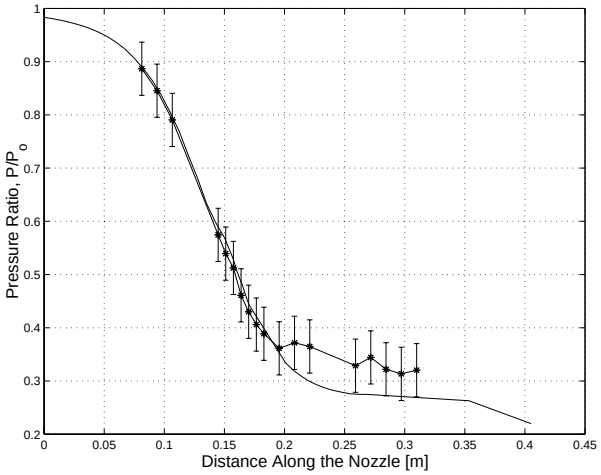

Figure 14: Pressure Ratio vs. Nozzle Length.

Here it is seen that the flow follows theory rather well up to pressure tap 12, where a divergence occurs. The boundary layer effects that were discussed earlier

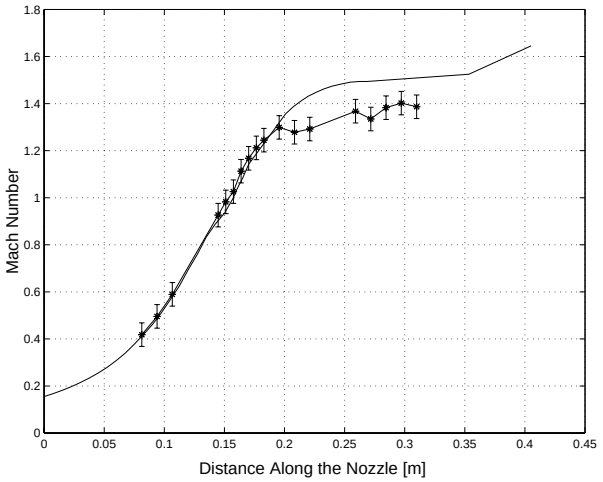

Figure 15: Mach Number vs. Nozzle Length.

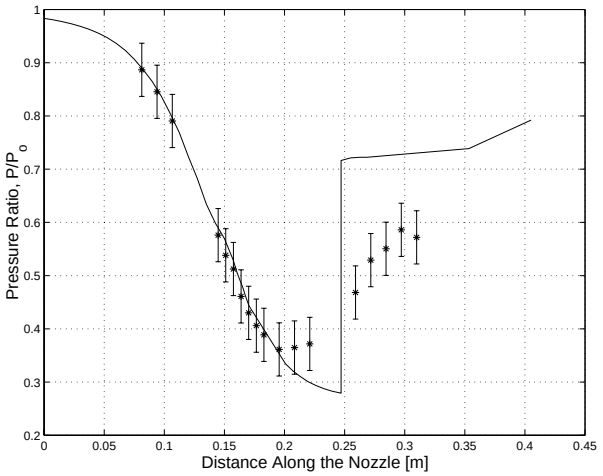

Figure 16: Pressure Ratio vs. Nozzle Length.

play a part in the divergence of the measured results from the theoretical results.

The particularly noticeable difference though is most likely caused by another factor. While that factor is not known for sure, it is speculated that the diverging portion of the nozzle played a role in combination with the boundary layer to disrupt the flow. Around the pressure tap where the differences compared to theory become large, the diverging section of the nozzle begins to diverge at a slower rate. Thus, it might be that the boundary layer growth overtakes the diverging area and a resulting area that the flow sees is smaller than the actual area of the wind tunnel. This would provide for some explanation to the discrepancy between the measured and theoretical values at the later pressure taps.

From the data given by the last pressure tap, $M_e = 1.39$ and $M_e = 1.387$ was calculated. The theoretical M_e was $M_e = 1.516$. The theoretical value is higher in this case, but for the same reasons as the theoretical subsonic values were lower than the measured values. Since flow velocity increases as area diverges when it is supersonic, and the theory is calculating M_e based on a larger area (not applying the boundary layer), it makes sense that the measured M_e is lower than the theoretical.

Shock Wave in the Diverging Section

Fig. 16 and Fig. 17 show the flow with a shock in the diverging section of the nozzle only, which was referred to previously.

As expected, the flow follows a nearly identical pattern as the supersonic design case up to the point where the shock wave occurs. At this point, there is a pressure rise, somewhere between pressure taps 13 and 14, and a sharp decrease in velocity. The velocity, as shown by calculations in Fig. 17, does not decrease to subsonic speeds until pressure tap 15 and the jumps across the shock wave do not completely reach the values predicted by theory. First, since the Mach number going into the actual shock wave was less than the theoretical shock wave, the jumps are going to be smaller. Also, as a second explanation, it is possible that the pitot tube begins to play a role in the flow and thus, adjusting the actual values that were measured. In the theoretical calculations, the pitot tube was ignored and assumed to not be present.

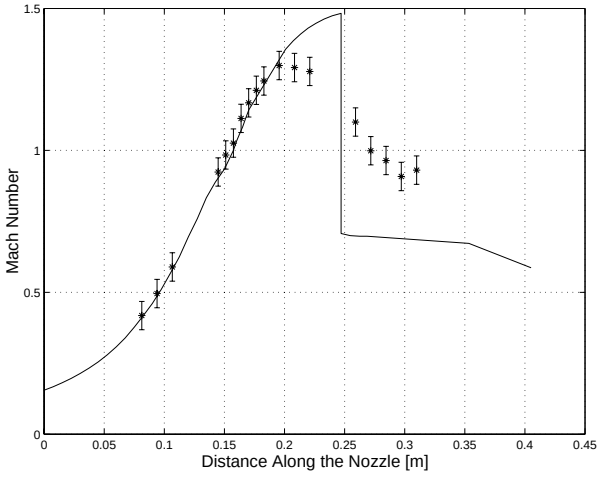

Figure 17: Mach Number vs. Nozzle Length.

The shock wave shown towards the right of Fig. 18 is the shock wave that occurred in the diverging section of the nozzle to produce the alteration in the flow that was found between pressure taps 13 and 14. Again, the shock is difficult to see, but the visualization was desired to help associate a physical picture with the studied phenomenon.

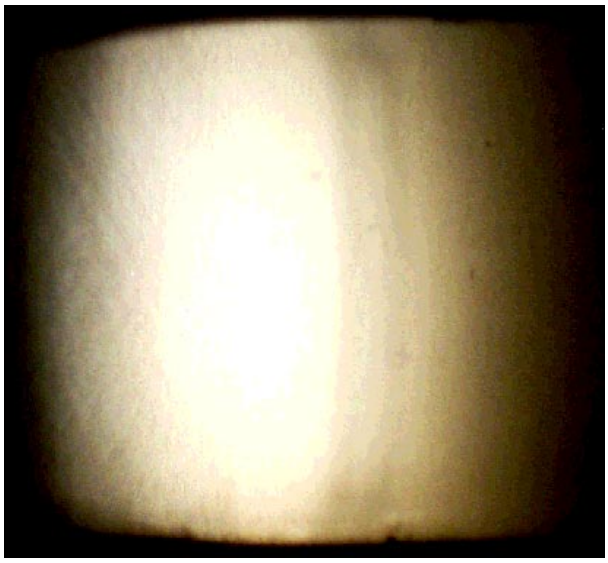

Figure 18: Shock Wave in the Diverging Section.

Also, the last pressure tap gave $M_e = 0.90$ and $M_e = 0.930$, while theory suggested $M_e = 0.562$. First of all, the pressure tap methods gave slightly more varied values of M_e than was found before. The unsteady nature of the shock probably contributed to this discrepancy even though the two values are reasonably agreeable. There is a much larger difference between the theory and the measured values, though. As was discussed before, the velocity drop across the shock was much weaker in the experiment as the velocity going into the shock was slower, this gives a higher value of M_e for the measured results.

Pitot Tube

When a pitot tube is placed in a supersonic flow, a normal shock occurs upstream. Consequently the pitot tube measures an increased pressure than the pressure would have been had the tube not been there. An illustration of the normal shock wave in front of the pitot tube can be seen in Fig. 19. Here, the Mach number just ahead of the shock is approximately 1.34. This is validated by both the experimental and theoretical data illustrated in the above section.

Cones

When the two cones of δ = 14° were secured in the test section, very similar results were produced. The difference in size between the two cones had little to no effect on the resulting shock system in the flow. This was expected, because the resultant flow around a cone or wedge is dependent not on the size of the body, but

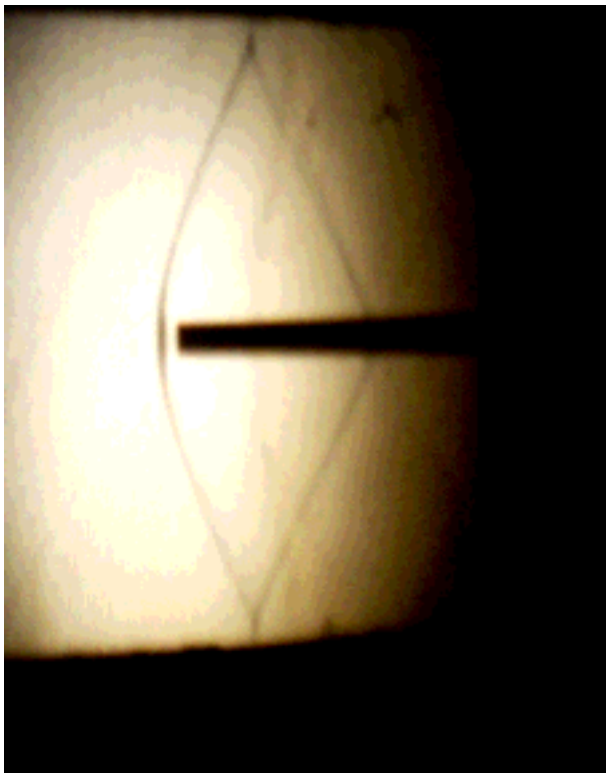

Figure 19: Shock Wave Formed Upstream of Pitot Tube.

on the deflection angle. Since both cones had identical deflection angles, it was understandable that the flow behaved similarly around them.

As seen in Fig. 20 and Fig. 21, the wave angles are identical. This wave angle β was measured to be approximately 52°. Using oblique shock relations,[4] it was determined that the Mach number just upstream of the cone was approximately 1.33.

This value matched well with the experimentally determined pressure data. The Mach number at the location of the tip of the cone based on the experimental and theoretical data from the pressure plots are similar. For the experimental data, the resulting Mach number for the small cone was approximately 1.38, and the Mach number for the larger cone was around 1.34. Both of these values match well with the geometrically determined Mach number.

The theoretically predicted Mach numbers were slightly higher, 1.50 and 1.49 for the small and large cone, respectively. The fact that these Mach numbers are slightly higher than the experimentally predicted Mach numbers can be understood when the effects of boundary layers in wind tunnel testing are considered. With the flow contracting slightly due to the development of boundary layers along the tunnel walls, the supersonic flow decelerates. This contributes to actual data yielding

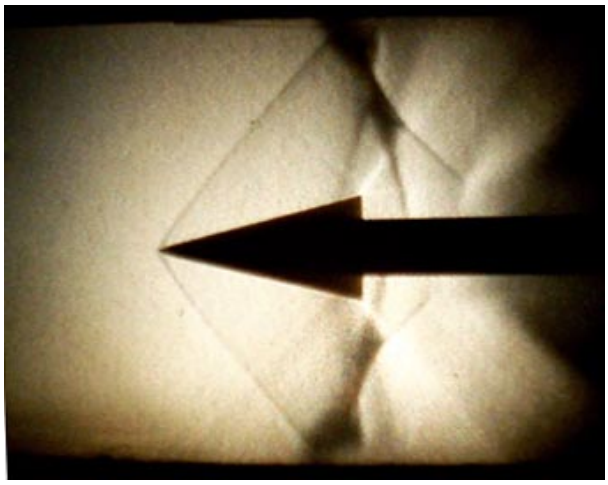

Figure 20: Large Cone, δ = 14°.

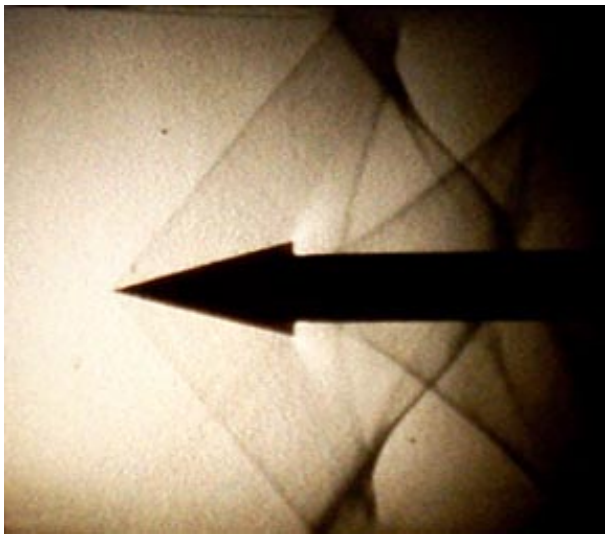

Figure 21: Small Cone, δ = 14°.

smaller Mach numbers than the theoretically predicted data.

Wedge Differences

Although cones and wedges are geometrically similar in that they both turn a flow through a deflection angle, their resulting effects on the flow can be quite different. If, for example, the cone used in this experiment was replaced with a wedge of identical δ, an oblique shock would not form. This is because the deflection angle of 14° is greater than the critical wedge angle for a flow of $M \approx 1.35$. The δ_{crit} for a flow of this Mach number is approximately 8°.

Because the deflection angle of the wedge would be greater than the critical deflection angle, a bow wave would be formed upstream of the wedge rather than an oblique shock. Behind this bow wave, the Mach number would be 0.762, and from isentropic and normal shock relations for the Mach number upstream of the shock of 1.35, the velocity can be determined. This was found to be 262 m/s.

Temperature Variations

Due to the fact that the stagnation temperature was measured through a metal tubing, there was a noticeable loss in temperature due to heat transfer. Because the flow around the tubing was traveling at high velocity, it inherently had a low temperature, significantly lower than the temperature in the tube. Some heat was lost through the tubing to the flow, and this is the reason for the discrepancy in ambient and measured stagnation temperatures shown in Fig. 22. If the plastic tubing would have been used, it would have performed as a much better insulator and would have reduced the heat loss and discrepancies between the two temperatures.

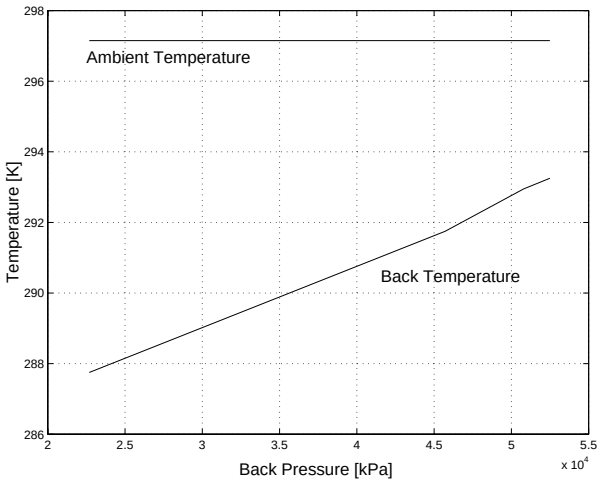

Figure 22: Variation of T and T_0 Through Tunnel.

Conclusions and Recommendations

An experiment using a convergent-divergent nozzle and schlieren flow visualization methods to analyze different shocks is presented. By varying the back pressure of the in-draft wind tunnel, the following flow regimes were analyzed: subsonic, sonic at the throat, sonic at the throat with a normal shock in the diffuser, and at the supersonic design condition.

While operating at the design condition, a pitot probe and two cones of similar geometry were placed in the flow. Using the schlieren method, these shocks and the shocks that occurred without a body in the test sec-

tion were captured for analysis. By measuring the wave angle β, an approximation of the Mach number could be made, and this value was compared to theory and experimentally acquired pressure data along the tunnel. A good correlation between experimental data and theory was established, with the theoretical Mach numbers higher or lower depending upon the type of flow and due to the growth of boundary layers along the tunnel walls.

The differences between wedges and cones of similar deflection angles were also analyzed. It was concluded that the critical deflection angle of a wedge is typically lower than that of a cone. This was based on the comparison of a wedge and a cone each with δ of 14°. It was found that while an oblique shock was formed by the cone, the wedge would have generated a bow wave, since the critical deflection angle for the Mach number was significantly less than the given deflection angle.

During the experimental test run, a great deal of noise could be heard. It was louder during the subsonic tests, because the noise and disturbances generated by the vacuum were able to propagate up the wind tunnel, since the flow was not greater than the speed of sound. It was interesting to note that during the supersonic tests, the noise level was less, but when the tunnel was shut off, there was a loud hissing sound as the flow decelerated to less than Mach 1, again illustrating the capability of the disturbances to propagate up the tunnel.

As for recommendations for future experiments, it would have been beneficial to have a better schlieren setup. It seemed that the angles of the lights and mirrors were constantly being changed throughout the experiment. Also, it was difficult to capture a good digital photograph because of the setup of the tripod. Further, if the plastic tubing had been tested as well as the metal tubing, a good comparison could have been made. Lastly, it would be interesting to know what specific values of back pressure were being utilized for the different flow regimes.

References

[1] National Geographic Home Page. “Chuck Yeager The Bell X-1,” National Geographic. <http://www.nationalgeographic.com/sound/speed.html> May 2001.

[2] NASA Dryden Home Page. “X-43,” NASA. <http://www.dfrc.nasa.gov/> May 2001.

[3] Falk, Eric A. and Asad Asghar, “Lab 6: Supersonic Flow in a Convergent-Divergent Nozzle.” Lab 6 Handout, May 2001.

[4] Oosthuizen, Patrick H. and William E. Carscallen, *Compressible Fluid Flow*, McGraw-Hill Inc., New York, 1997.

[5] Anderson, John D., *Introduction to Flight*, 3rd Ed., McGraw-Hill Inc., Boston, MA, 1989.

[6] Kuethe, Arnold M. and Chuen-Yen Chow, *Foundations of Aerodynamics*, 5th Ed., John Wiley Sons, Inc., New York, 1998.

[7] Dunn, Patrick F., *Fundamentals of Measurements and Data Analysis*, 4th Rev., Notre Dame, IN, 2000.

[8] Falk, Eric A. and Eric J. Jumper, “Upstream-Propagating Potential Waves Elicited From the Stator Row Downstream of a Fan,” AIAA paper number 99-2805.

Appendix A: Uncertainty

The uncertainty for this experiment was rather straightforward. The uncertainties in the pressures and temperatures should have been simply the precision error that was associated with taking the measurements. However, another type of error was discovered during the performance of the experiment. It was noticed that in the tubes of mercury with which the pressure was being taken, there were masses of ash and dust that had built up in the measurement devices. There was no exact way to quantify the error associated with this debris, so a value was assumed and included in the pressure error that was used. Because the precision error and the debris error were both the same for all the pressures measured, the overall pressure error was also the same because it was just a sum of the two separate errors.

The error in the Mach number calculations was not difficult once the base quantities’ errors were known. Using the method of partial differentiation, the errors in the base measurements were carried through the rest of the calculations resulting in the desired Mach number errors.

Figure 23: Group 5.